First-Step Anodization of Commercial Aluminum in Oxalic Acid: Activation Energy of Rate Process and Structural Features of Porous Alumina and of Aluminum Substrate as a Function of Temperature

[1]Syed Muhammad Junaid Zaidi and [2]Muhammad. Zakria Butt*

[1]*Department of Physics, GC University, Lahore-54000, Pakistan.*

[2]*Centre for Advanced Studies in Physics, GC University, Lahore 54000, Pakistan.*

mzakriabutt@gmail.com*

(Received on 23rd November 2017, accepted in revised form 26th May 2018)

Summary: First-step anodization of commercial aluminium was carried out in 0.3 M oxalic acid at five temperatures –10, –5, 0, 5, and 10 ºC, keeping the anodization voltage (40 V) and time (15 min) constant. It is found that the current density, charge transferred, and thickness of porous alumina film increase exponentially with anodization temperature. The activation energy of the rate process of anodization determined from the Arrhenius plots of current density, charge transferred, and film thickness is found to be 0.357 eV with a standard deviation of 0.013 eV. Structural features of the porous alumina examined by SEM show that the pore diameter, interpore distance, and porosity increase whereas pore circularity and pore density decrease linearly with the increase in anodization temperature. Moreover, XRD studies of the anodized commercial aluminum substrate show that the intensity of diffraction peak pertaining to preferentially oriented crystallographic plane (311) is decreased whereas its full width at half maximum is increased at all anodization temperatures.

Keywords: Anodic aluminum oxide; Film thickness; Activation energy of rate process; SEM; XRD; Structural features.

Introduction

In the last few decades, the porous anodic aluminum oxide (AAO) films have attracted much attention for the fabrication of nanostructured materials. Such films are formed on aluminum substrate by the process of electrochemical anodization. The electrolyte used for this purpose can be acidic, e.g. oxalic acid, sulfuric acid, and phosphoric acid [1–3], etc or basic, e.g. sodium hydroxide [4] etc. It is well known that the porous AAO films possess good mechanical, thermal, and chemical stability, excellent dielectric properties, and controllable pore diameter as well as interpore distance. Their diverse applications include biosensors fabrication, hemodialysis devices, nanopores template, conductive substrate, supercapacitors [5–9], etc.

To grow metal oxide films on a pure metal surface, several anodization methods have been adopted, namely one-step or mild anodization at low voltage [10], two-step anodization [11], hard anodization at low temperature and high voltage [3], pulsed anodization [12], and plasma anodization [13], etc. The growth of the porous AAO film depends on various anodization parameters involved in the experiment, like anodization voltage, time, and temperature [11, 14, 15] as well as concentration and nature of electrolyte [16].

The temperature of the electrolyte at which anodization of metals is carried out influences not only the thickness of the oxide layer but also its structural features. For instance, Sulka and Stepniowski [17] studied the effect of relatively high temperatures (20, 25, 30 $^{\circ}$C) on the anodization of 5N+ pure aluminum in 0.3M oxalic acid ($C_2H_2O_4$) at different anodizing voltages in the range 30 – 65 V with an interval of 5 V. The time of anodization of a given specimen was either 30 or 60 min. They found that for a given anodizing voltage and time, various parameters namely the current density, oxide layer thickness, pore diameter, interpore distance and porosity increase with temperature whereas pore density decreases. Moreover, Stepniowski and Bojar [11] developed nanoporous alumina by anodization of 5N+ pure aluminum in 0.3M oxalic acid at still higher temperatures (35, 40, 45, 50 $^{\circ}$C) for different anodizing voltages ranging from 20 to 60 V with an interval of 5 V. For each anodizing voltage, the time of anodization of the specimens was 30, 60, and 120 min. They again found that the structural parameters referred to above, except interpore distance, followed the same trend for each anodizing voltage and time. However, the interpore distance was significantly influenced only by the anodizing potential, and remained almost independent of anodizing temperature or duration of anodization.

*To whom all correspondence should be addressed.

Likewise, Kashi and Ramazani [18] investigated the effect of anodization temperature (0 °C – 25 °C) on the self-organized pore formation in anodic alumina. They used 5N pure aluminum as substrate in 0.3 M oxalic acid and anodization voltage was 40 V. They observed that the variation of current density J with anodization temperature T followed a typical exponential relation:

$$J = J_o \exp(-E/kT) \quad (1)$$

where E is the activation energy of the rate process of anodization and k is the Boltzmann constant. The value of E = 0.44 ± 0.01 eV measured by Kashi and Ramazani [18] for anodization of 5N pure aluminum at 40 V is about two times higher than that (E = 0.182 ± 0.007 eV) measured by Zaidi and Butt [19] for anodization of commercial purity aluminum at 50 V. The difference may be attributed to the fact that anodization voltage (50 V) used by Zaidi and Butt [19] is higher than that (40 V) used by Kashi and Ramazani [18]; higher anodization voltage facilitates the anodization process and therefore reduces the activation energy E of the rate process of anodization.

The basic purpose of the present research work was to compare the first-step anodization response of commercial purity aluminum with that of 5N+ high-purity aluminum in an electrolyte of 0.3M oxalic acid for a constant anodization voltage. The main features of interest are the activation energy of the rate process of anodization as well as various structural features of porous alumina film, namely the pore diameter, interpore distance, pore circularity, pore density, and porosity, etc. Another objective was to explore the structural modifications occurred in the aluminum substrate on anodization, not reported in the literature before.

Experimental

Six square shaped specimens (1.5 cm × 1.5 cm) of 1 mm thickness were cut from an aluminum sheet. The specimens were pre-heated at 450°C for 3 hours to remove internal stresses. After mechanical polishing, the specimens were electro-polished in a mixture of perchloric acid ($HClO_4$) and C_2H_5OH with a proportion of 1:4 by volume at a constant current density of 500 mA cm^{-2} for 2 min at 10 °C. Five specimens were then anodized in an electrolyte of 0.3M oxalic acid ($C_2H_2O_4$) in an anodization chamber at 40 V for 15 min at five different temperatures, namely –10, –5, 0, 5, and 10 °C, and the sixth specimen was kept un-anodized for later usage as reference. The electrolyte was stirred vigorously during anodization for uniform temperature distribution. The value of current was recorded during the experiment at each temperature via computer interfaced multimeter. Detailed specifications of the equipments employed in the electrochemical anodization setup are given in [19].

Results and Discussion

Current – time response

Fig. 1 represents current – time plots of aluminum specimens anodized at – 10, – 5, 0, 5, and 10°C. One can see that after a sudden increase in current due to the movement of electrolyte ions towards anode on the application of voltage, the current is then sharply decreased due to an oxide layer formed on the specimen surface, and is later on stabilized due to equilibrium between oxidation and reduction process during anodization. It is worthy of mention that the current – time plot of specimen anodized at 10°C represent rather large distortion in current after 150 s, which means that that there is some irregularity in the process of oxidation and reduction or the pores formation process is not uniform. Reference to Fig. 1 also shows irregular behavior of current at anodization temperature of 5°C. The reason is that during anodization heat generates due to the movement of ions towards the anode. Slightly before 300 s, the oxidation process dominates over reduction process, and the number of ions involved in the movement towards anode progressively increases. At -10 °C irregularity in the curve was observed after 150s and 500s which is due to the irregularity between oxidation and reduction process. The smooth behavior of the curve was observed at 0 °C.

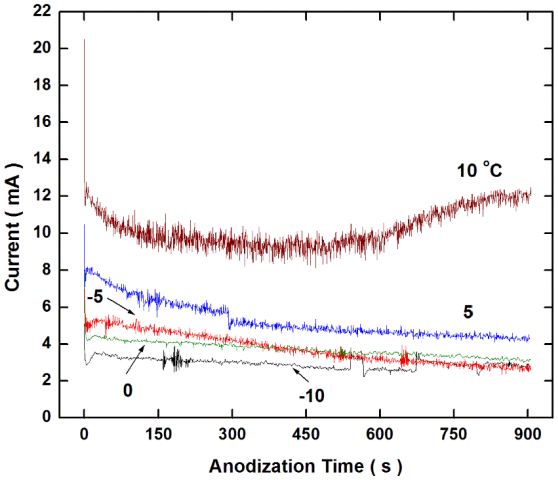

Fig. 1: Current – time plots of aluminum specimens anodized at –10, –5, 0, 5, and 10 °C.

Current density versus anodization temperature

Current density of anodization is defined as the ratio of the total current involved in the anodization process and the area of the specimen being anodized. The points in Fig. 2 (a and b) denote the values of current density *J* and total charge transferred *Q*, respectively, as a function of anodization temperature. The lines drawn through the data points by least-squares fitting method represent an exponential growth in each case. It shows that mobility of electrolyte ions increases rapidly with anodization temperature between 0 to 10˚C.

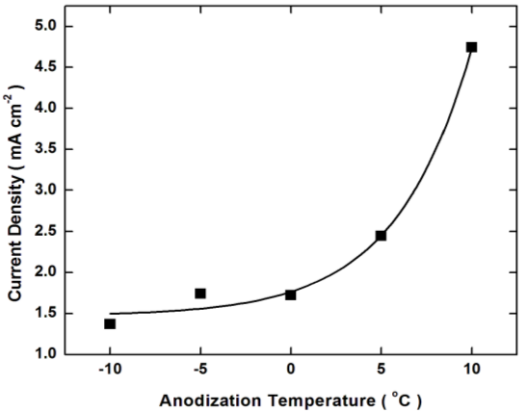

(a)

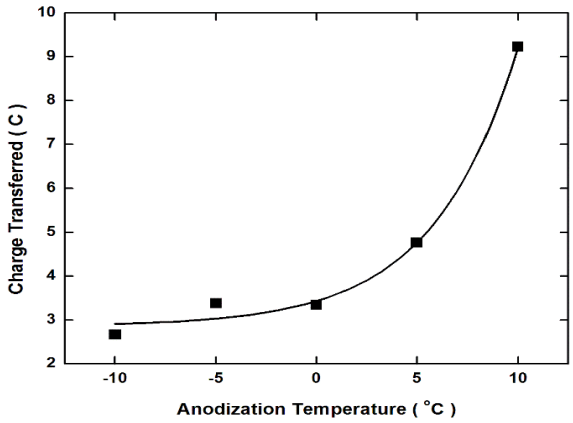

(b)

Fig. 2: Dependence of anodization current density (a) and charge transferred (b) on the temperature of 0.3 M oxalic acid electrolyte.

Film thickness analysis

The film thickness of anodized specimens was calculated from Faraday's Law [20, 21]:

$$d = \frac{QM}{xy\,\rho\,FA} \quad (2)$$

Here *d* is the thickness of anodized film, *Q* is the amount of charge passed, *M* (= 101.96 g mol^{-1}) is the molecular mass of Al_2O_3, *x* is the number of Al^{+3} ions in Al_2O_3 molecule, *y* is the number of O^{-2} ions in Al_2O_3 molecule, ρ (= 3.95 g cm^{-3}) is the density of Al_2O_3, *F* (= 96485 C mol^{-1}) is Faraday's constant, and *A* (= 2.16 cm^2) is the anodized area of the specimen. The values of film thickness (μm) of anodized specimens calculated by equation (1) have been denoted by points in Fig. 3(a) and Fig. 3(b) as a function of anodization temperature and total charge transferred, respectively. Least-squares fitting method was used to pass lines through the data points in each case. It is evident that the film thickness increases exponentially with anodization temperature and linearly with charge transferred. Moreover, the growth rate (nm min^{-1}) of thin films was calculated from Faraday's Law, and was plotted as a function of current density *J* (mA cm^{-2}) in Fig. 3(c). A linear fit to the data points by least-squares fitting method shows that the growth rate of anodized films is directly proportional to the current density.

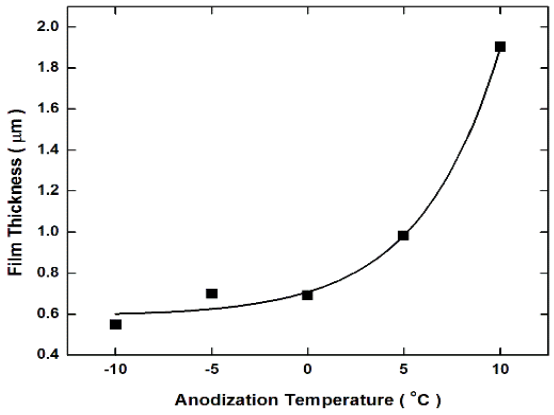

(a)

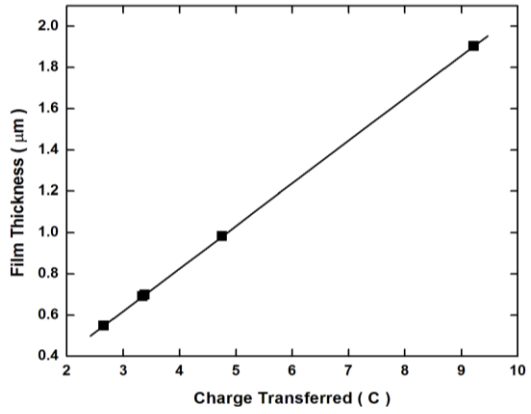

(b)

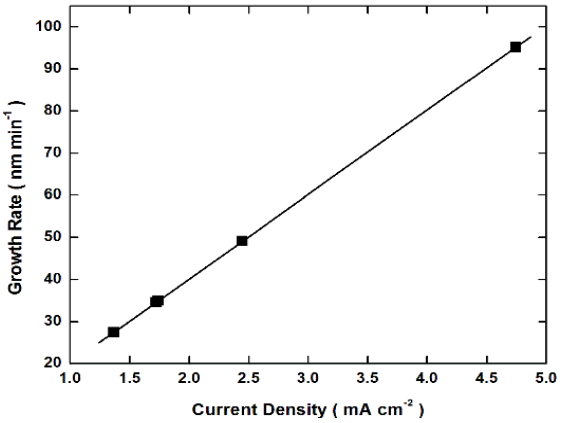

(c)

Fig. 3: Film thickness as a function of (a) anodizing temperature and (b) charge transferred. (c) Growth rate of anodized film as a function of current density.

Rate process of anodization

To determine the activation energy of the rate process of anodization, the data pertaining to current density *J*, charge transferred *Q*, and film thickness *d* have been plotted as a function of the inverse of anodization temperature T^{-1} in log-linear coordinates in Fig. 4. The straight lines fitted to data points in each case by least-squares fitting method are given by the following expressions:

$$\ln J = 16.55 - 4307\ T^{-1} \quad (3)$$

$$\ln Q = 16.10 - 4000\ T^{-1} \quad (4)$$

$$\ln d = 14.99 - 4135\ T^{-1} \quad (5)$$

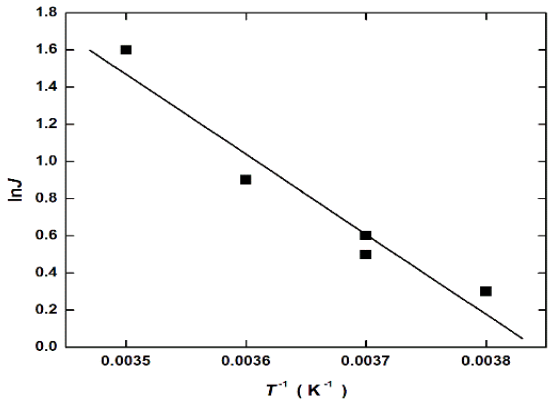

(a)

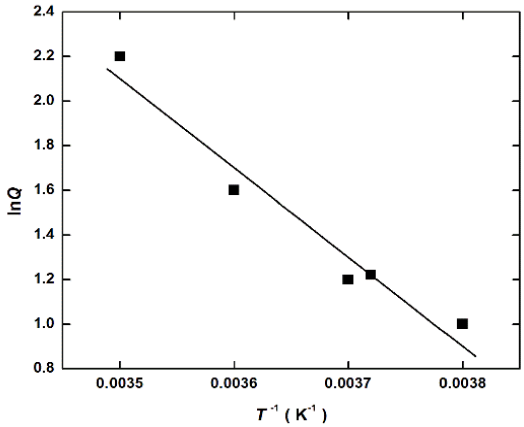

(b)

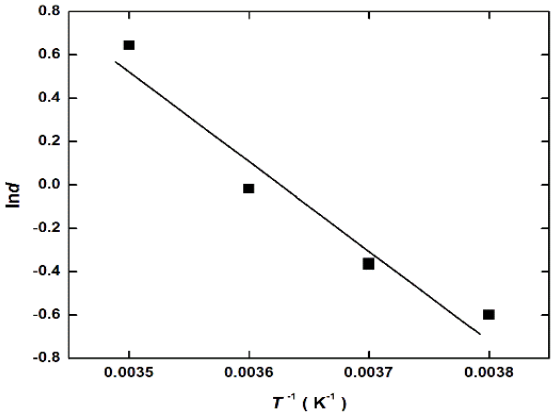

(c)

Fig. 4: Arrhenius plots of (a) current density *J*, (b) charge transferred *Q*, and (c) film thickness *d* of anodized aluminium.

with linear correlation coefficient $r = -0.984$, -0.989, and -0.986, respectively. The activation energy *E* of the rate process is found to be 0.357 eV with a standard deviation of 0.013 eV. This is in reasonable agreement with the value of *E* (0.44 ± 0.01 eV) measured by Kashi and Ramazani [18] for anodization of 5N pure aluminum in 0.3 M oxalic acid at 40 V.

SEM analysis

The surface morphology of aluminum specimens anodized at (a) −10, (b) − 5, (c) 0, (d) 5, and (e) 10 ºC was studied by scanning electron microscope (Model: JSM-6480 LV, JEOL). SEM top-view image micrographs are given in Fig. 5. Various structural parameters, namely the pore diameter (D_P), interpore distance (D_i), pore density (*n*), pore circularity, and porosity (*P*) were measured from these micrographs with the help of Image J software.

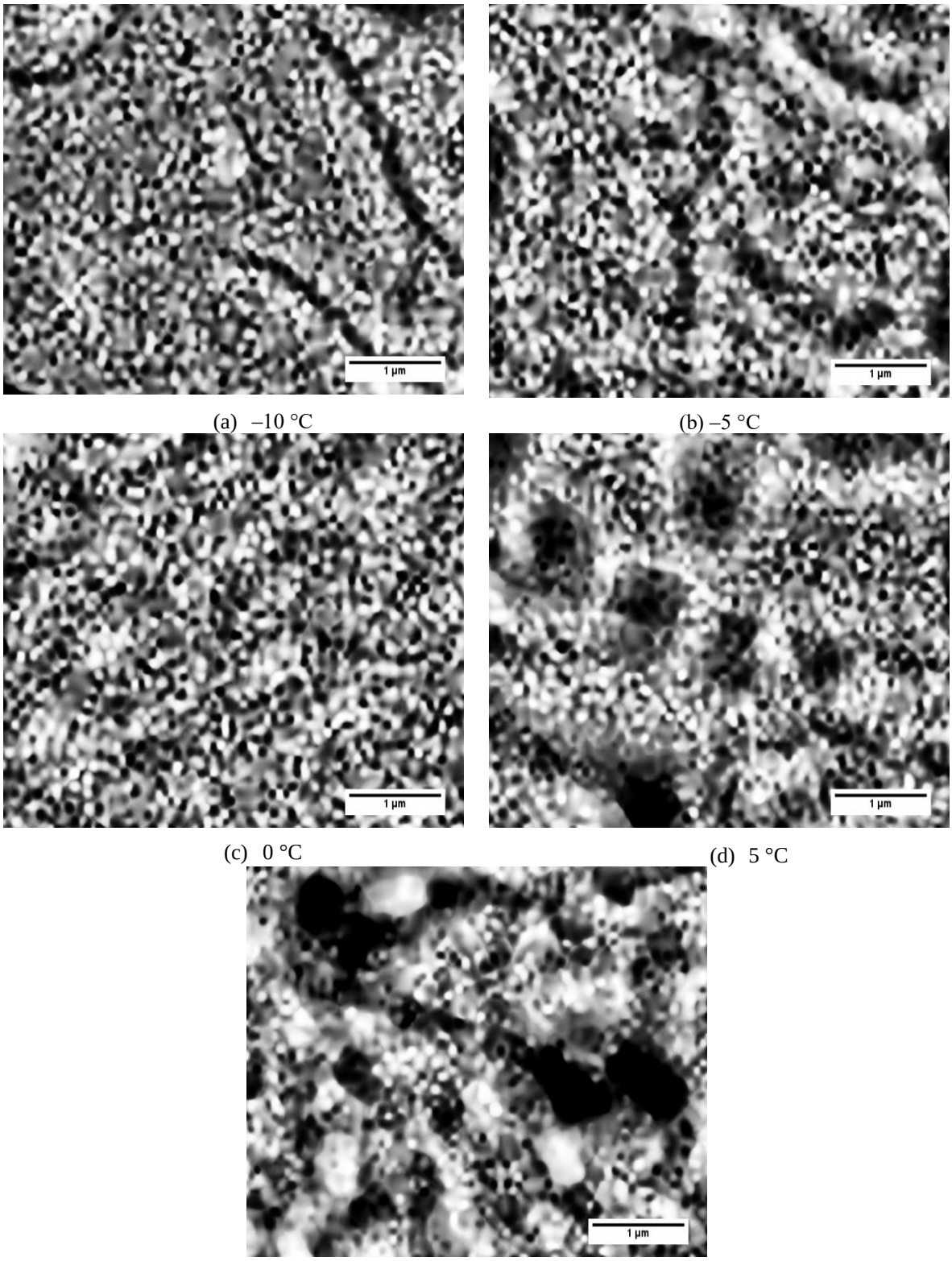

(a) –10 °C (b) –5 °C

(c) 0 °C (d) 5 °C

(e) 10°C

Fig. 5: SEM top-view micrographs of porous alumina layer formed at various anodization temperatures: (a) –10 °C, (b) –5 °C, (c) 0 °C, (d) 5 °C, and (e) 10 °C.

Referring to Fig. 6(a) and Fig. 6(b), pore diameter (D_P) increases linearly from 88 to 110 nm and interpore distance (D_i) increases from 132 to 148 nm with the increase in anodization temperature in the range – 10 ºC to + 10 ˚C. Besides pore size, pore circularity is also an important factor for porous anodic aluminum oxide film. It is defined as [10]:

$$Circularity = 4\pi \frac{A}{s^2} \quad (6)$$

Here *A* and *s* are area and perimeter of each pore. If circularity is 1, the pore shape is a perfect circle. The pore circularity is found to increase from 0.82 to 0.91 with the rise in temperature of electrolyte, as is evident from Fig. 6(c). One can also readily find pore density by means of the mathematical expression [22]:

$$n = \frac{2\times10^6}{\sqrt{3}\times D_i^2} \quad (7)$$

It is evident from Fig. 6(d) that pore density decreases linearly from 66.2 to 52.0 μm^{-2} with the increase in anodization temperature of electrolyte. It points to progressive merging of pores as anodization temperature is increased from – 10 to + 10 ºC. Using the values of pore diameter (D_P) and interpore distance (D_i), one can determine the porosity (*P*) of the aluminum oxide film from the formula [22]:

$$P = 0.907 \left(\frac{D_p}{D_i}\right)^2 \quad (8)$$

Reference to Fig. 6(e) shows that porosity (*P*) of the aluminum oxide film increases from 40% to 50% as anodization temperature is increased from – 10 to + 10 ºC. Finally, a comparison of Figs. 6(a), (b) and (d) shows that an increase in pore diameter and interpore distance is accompanied by a decrease in pore density. Zhang *et al* [23] have explicitly shown that circularity, regularity, and sharpness of the pores developed during first-step anodization of aluminum substrate improve on second-step anodization under the same anodization conditions.

Structural characterization of anodized aluminum substrate

XRD patterns of un-anodized and anodized aluminium specimens are shown in Fig. 7(a). All the noticeable peaks, on comparison with the standard reference pattern (JCPDS: 01-089-4037), were indexed as (111), (200), (220), and (311).

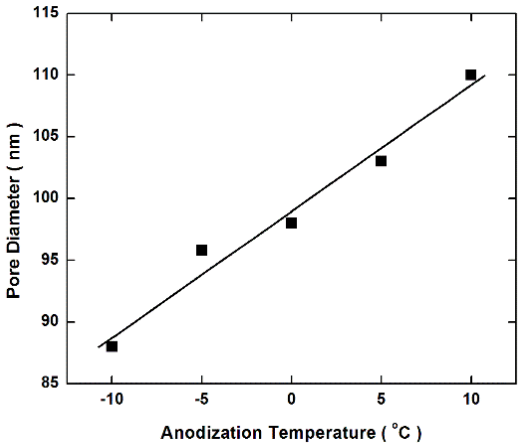

(a)

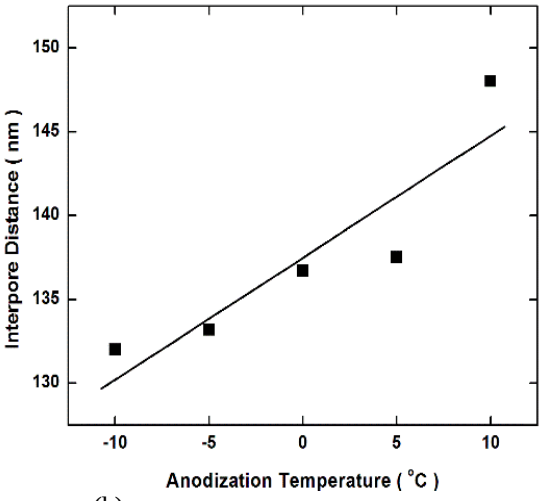

(b)

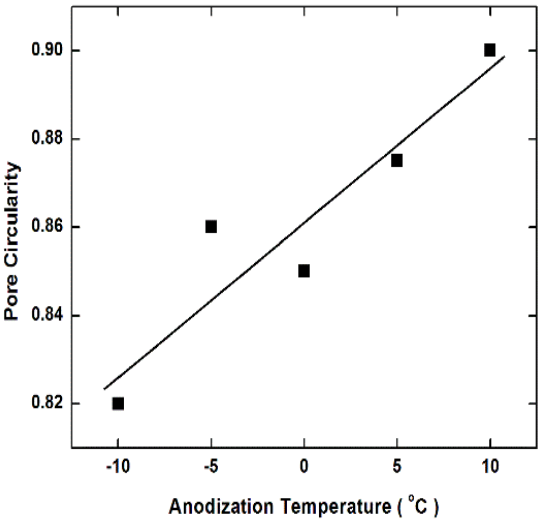

(c)

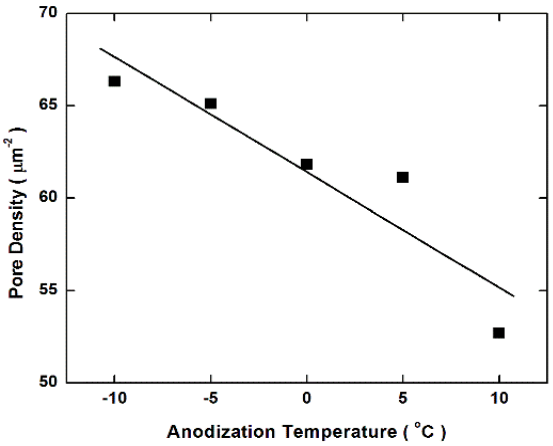

(d)

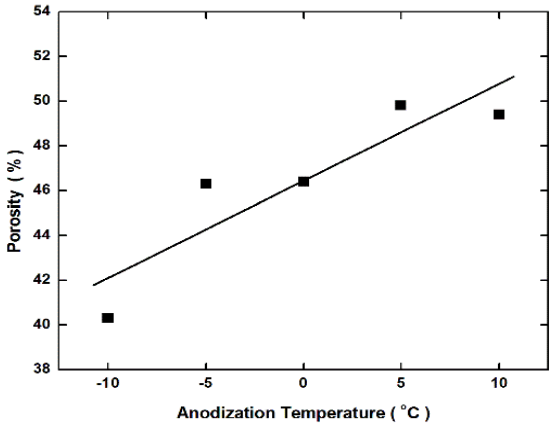

(e)

Fig. 6: Pore diameter (a), interpore distance (b), pore circularity (c), pore density (d), and porosity (e) as a function of anodization temperature

To determine the preferred orientation of un-anodized Al specimen, Harris analysis was performed using the following formula of texture coefficient [24, 25]:

$$P(h\ k\ l) = \frac{I(h\ k\ l)}{I_o(h\ k\ l)}\left[\frac{1}{n}\sum_{i=1}^{n}\frac{I(hkl)}{I_o(hkl)}\right]^{-1} \qquad (9)$$

Here I is the observed relative intensity with respect to the most intense diffracting plane and I_o is the standard relative intensity for (h k l) planes obtained from the JCPDS Card No. 01-089-4037 and n is the number of peaks in the diffraction pattern. For preferentially oriented plane, the P (h k l) value should be greater than 1 [24, 25]. The texture coefficient of all four diffracting planes of un-anodized Al specimen obtained in this manner has been plotted as a function of 2θ in Fig. 5(b). One can readily see that the value of texture coefficient pertaining to (220) and (311) planes is greater than 1, while it is less than 1 for (111) and (200) planes.

Moreover, the points in Fig. 7(c) represents the peak intensity of preferentially oriented (311) plane of five anodized aluminum specimens as a function of anodization temperature. The horizontal dash line represents the peak intensity level of (311) plane of un-anodized aluminum specimen. Suffice to say that the peak intensity of (311) plane of un-anodized aluminum specimen is considerably decreased on anodization. According to simulation studies of Makinson *et al* [26], the peak intensity of x-rays diffraction peak of a crystallographic plane depends on the concentration of point defects in it. As the concentration of point defects (e. g. vacancies) increases, the peak intensity decreases. This points to the amorphous nature of the anodized film formed on the aluminum specimens.

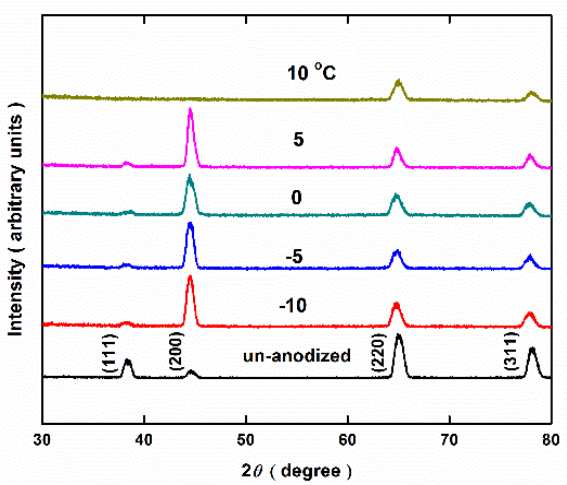

(a)

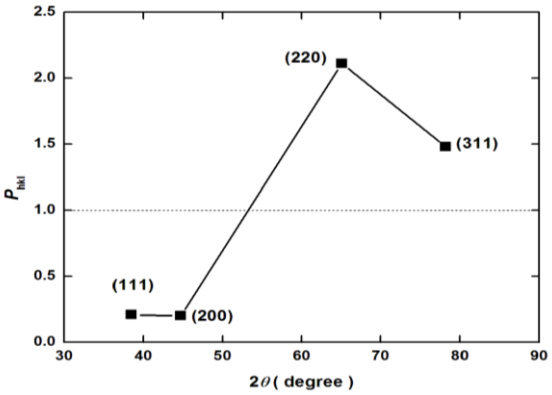

(b)

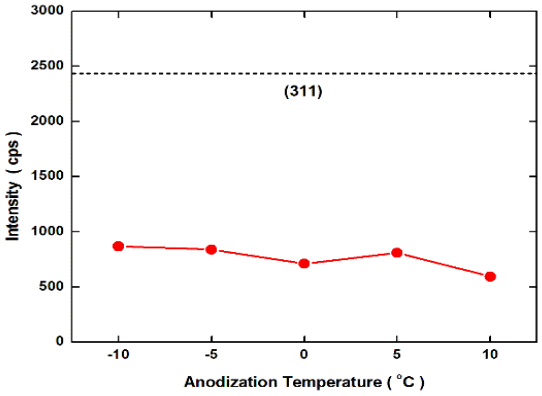

(c)

Fig. 7: (a) Combined XRD patterns of un-anodized and anodized aluminum specimens, (b) texture coefficient of various crystallographic planes of un-anodized aluminum specimen, and (c) peak intensity of preferred orientation plane (311) as a function of anodization temperature.

X-ray diffraction peaks broadening is caused by crystallite size (i.e. average size of coherently diffracting domains) and lattice strain, which can be analyzed by Williamson and Hall method [27, 28]. The mathematical expression for the full width at half maximum (FWHM) of diffraction peak can be written as:

$$\beta = \beta_D + \beta_\varepsilon, \qquad (10)$$

Here β_D and β_ε are contributions to FWHM by crystallite size D and lattice strain ε, respectively. The peak broadening due to crystallite size D is given by Scherrer formula:

$$\beta_D = \frac{k\lambda}{D\cos\theta} \qquad (11)$$

Here λ is x − ray wavelength (= 0.15406 nm for CuK_α radiation) and $k \approx 0.9$ is shape factor. Contribution towards peak broadening by lattice strain ε is given by Wilson formula:

$$\beta_\varepsilon = 4\varepsilon \sin\theta \qquad (12)$$

The FWHM of a diffraction peak is then given by the following expression:

$$\beta = \frac{k\lambda}{D\cos\theta} + 4\varepsilon\tan\theta \qquad (13)$$

Or

$$\beta\cos\theta = \frac{k\lambda}{D} + 4\varepsilon\sin\theta \qquad (14)$$

This is known as Williamson – Hall equation. One can also re-write equation (14) in an alternate form as

$$\beta\cos\theta = A + B(4\sin\theta) \qquad (15)$$

where A (= $k\lambda/D$) and B (= ε) are dimensionless constants.

Figs. 8(a) – (f) portray Williamson-Hall plots of un-anodized and anodized aluminum specimens for various anodization temperatures in the range –10 ºC to +10 ºC. The straight lines passed through the data points by least-squares fitting method are in accord with equation (15). The values of intercept A (= $k\lambda/D$) on y-axis and slope B (= ε) determined in this manner in each case are given in Table-1.

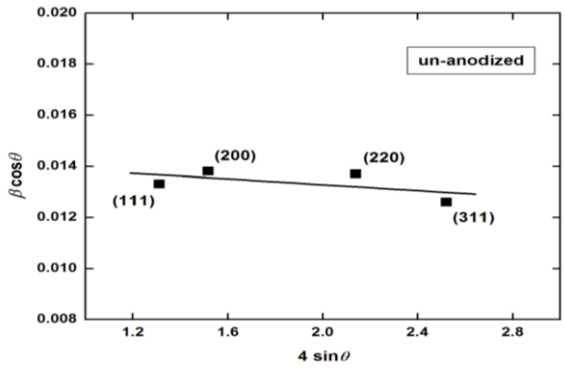

(a)

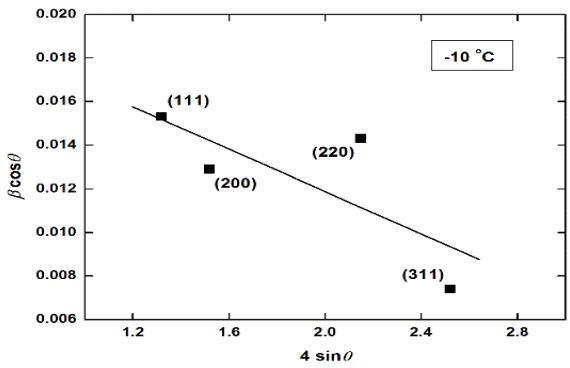

(b)

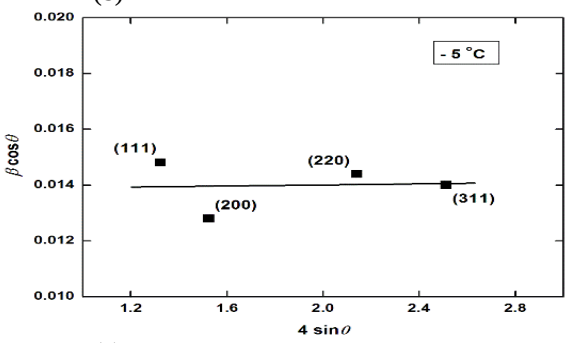

(c)

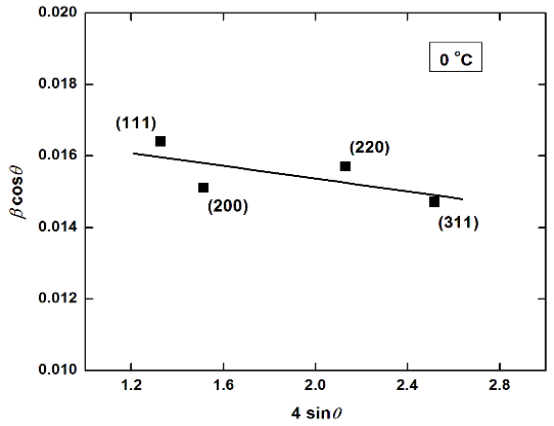

(d)

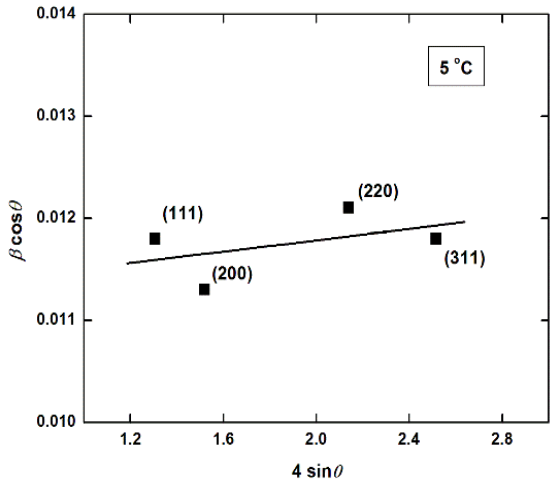

(e)

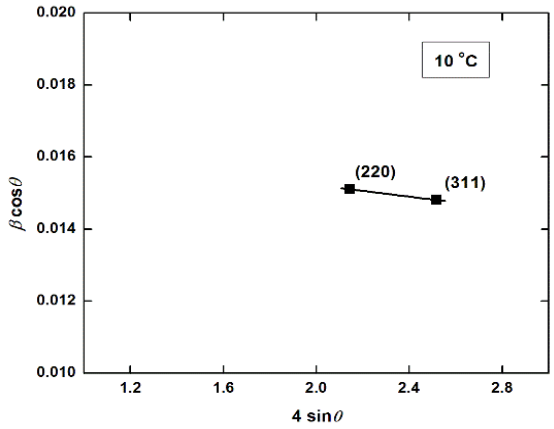

(f)

Fig. 8: Williamson – Hall plots of un-anodized and anodized aluminum specimens for various anodization temperatures in the range –10 °C to 10 °C.

Table-1: Structural data of aluminum substrate obtained by Williamson – Hall analysis.

T (°C)	*A*	*B* (= ε)	*D* (nm)
Un-anodized	0.01440	-0.00560	9.63
-10	0.02157	-0.00490	6.42
-5	0.01382	-0.00009	10.05
0	0.01715	-0.00089	8.06
5	0.01124	0.00030	12.38
10	0.01682	-0.00080	8.25

The values of crystallite size *D* and lattice strain *ε* (Table-1) of anodized aluminum specimens have been depicted by points as a function of anodization temperature in Fig. 9(a) and Fig. 9(b), respectively. One can readily see that crystallite size *D* follows an increasing trend with anodization temperature though small. However, lattice strain *ε* first increases rapidly and then remains almost invariant with temperature in the range – 5 °C to +10 °C. The nature of lattice strain *ε* is compressive (–) for all the anodization temperatures, except for 5 °C which is tensile (+). The interdependence of *D* and *ε* has been illustrated in Fig. 9(c). Sigmoidal fit to the data points in Fig. 9(c) shows that lattice strain increases with the increase in crystallite size.

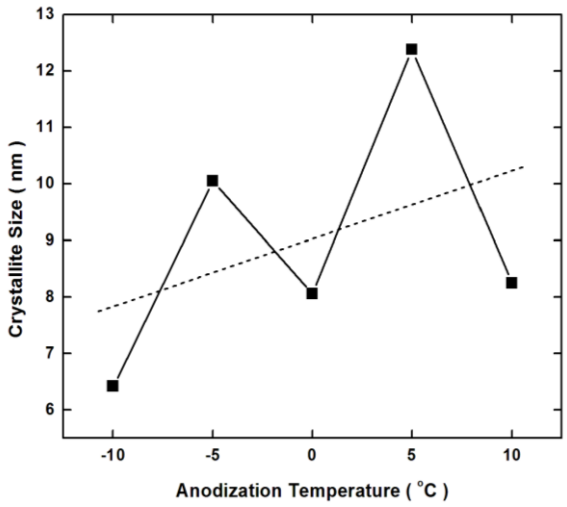

(a)

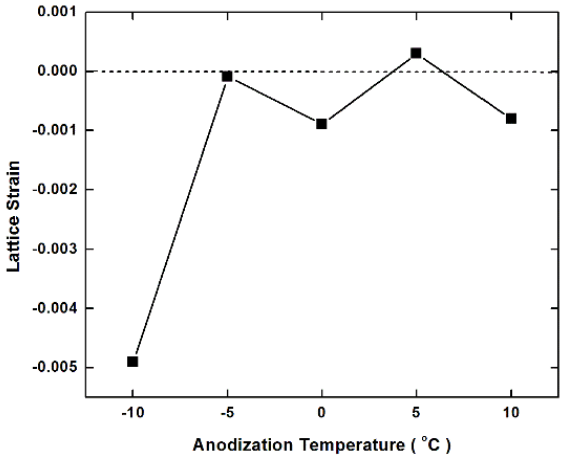

(b)

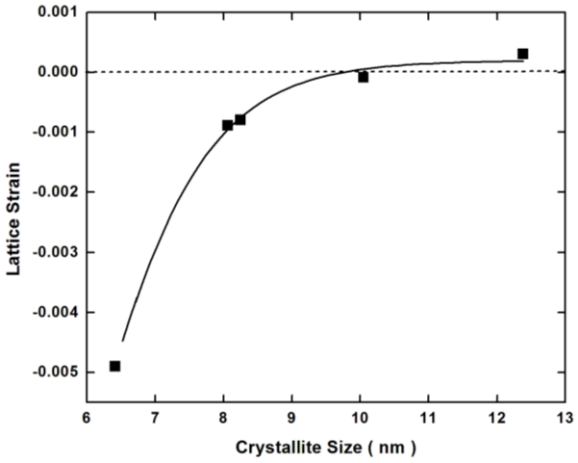

(c)

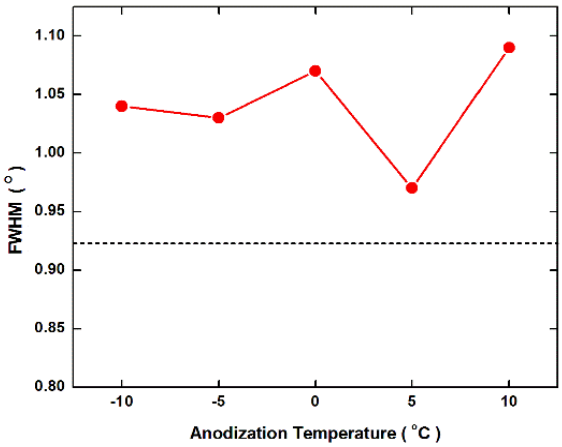

(d)

Fig. 9: (a) Crystallite size and (b) lattice strain as a function of anodization temperature, (c) relationship between lattice strain and crystallite size, and (d) FWHM of (311) diffraction peak as a function of anodization temperature

The profiles depicted in Figs. 9(a) – (c) are not unusual but similar to the ones reported in [29, 30]. Butt *et al* [29] have observed that irradiation of Al5086 alloy specimens in vacuum with 248 nm – 20 ns KrF excimer laser produces structural changes in the specimens. Both the crystallite size *D* and lattice strain ε increase as the number of laser shots are increased from 100 to 500. In fact, on laser – material interaction the light energy is converted into the heat energy; higher the number of laser shots more is the heat energy produced. This causes a progressive increase in the crystallite size *D* and lattice strain ε with the number of laser shots. Similarly, Khaliq *et al* [30] have found both the crystallite size *D* and lattice strain ε in zinc single crystal specimens when irradiatied with 500 keV singly – charged carbon ions show a decreasing trend with the increase in ion dose from 3.94×10^{14} ions cm^{-1} to 130×10^{14} ions cm^{-1}. This structural change is caused by the energy of the ions given up to the lattice by collisions before coming to rest. Likewise, the profiles portrayed in Figs. 9(a) – (c) originate from the heat energy produced during the electrochemical anodization process. Higher the anodizaton temperature (-10 ºC to 10 ºC) more is the heat energy absorbed by the aluminum substrate. The interdependence of the crystallite size *D* and lattice strain ε (Fig. 9(c)) is also similar to the one reported in [19, 29, 30].

Finally, points in Fig. 9(d) denote the values of FWHM of diffraction peaks of preferentially oriented (311) plane of five anodized aluminum specimens as a function of anodization temperature. The horizontal line at 0.92º level represents the FWHM of (311) plane of un-anodized aluminum specimen. Suffice to say that the FWHM of (311) plane of un-anodized aluminum specimen is increased on anodization by 12 to 21%. According to Ungar [29], x-ray diffraction peaks are broadened if lattice defects, e.g. point defects like vacancies, are considerably increased. This trend is consistent with the observations portrayed in Fig. 7(c) that the peak intensity of preferentially oriented (311) plane of five anodized aluminum specimens decreases with the increase in anodization temperature due to increase in the concentration of point defects in it. Thus a decrease in the peak intensity of x-rays diffraction peak of a crystallographic plane due to increase in vacancy concentration is accompanied by an increase in FWHM or peak broadening of the diffraction peak.

Conclusions

The investigations pertaining to the first-step anodization of commercial aluminium carried out in 0.3 M oxalic acid at different temperatures, namely –10, –5, 0, 5, and 10 ºC, for a given anodization voltage (40 V) and time (15 min) lead to the following conclusions.

1. The current density (1.37 mA cm^{-2} – 4.74 mA cm^{-2}), charge transferred (2.66 C – 9.22 C), and thickness of porous alumina film (0.55 µm – 1.90 µm) increase exponentially with the anodization temperature.
2. The activation energy of the rate process of anodization determined from the Arrhenius plots of current density, charge transferred, and film thickness is found to be 0.357 eV with a standard deviation of 0.013 eV.
3. Structural features of porous alumina examined by SEM show that the pore diameter (88 nm to

110 nm), interpore distance (132 nm – 148 nm), and porosity (40% – 50%.) increase whereas pore circularity (0.821 – 0.912) and pore density (62.2 μm^{-2} – 52.0 μm^{-2}) decrease linearly with the increase in anodization temperature.

4. XRD studies of anodized commercial aluminum substrate reveal that the intensity of diffraction peak pertaining to preferentially oriented crystallographic plane (311) is decreased whereas its FWHM is increased at all anodization temperatures.
5. The observations are in good agreement with those reported in the literature for high-purity aluminum.

Acknowledgement

One of the authors (S. M. J. Zaidi) is grateful to the Higher Education Commission, Islamabad for financial assistance under the Indigenous PhD 5000 Fellowship Program Phase-3. Authors are also grateful to the referee for his constructive criticism and valuable suggestions.

References

1. G. D. Sulka and K. G. Parkoła, Temperature influence on well-ordered nanopore structures grown by anodization of aluminum in sulphuric acid, *Electrochim. Acta.*, **52,** 1880 (2007).
2. Y. Zuo, Y. Zhao, X. Li, N. Li, X. Bai and S. S. Qiu, Synthesis of nanowire and nanorods by anodic oxidation method, *Mater. Lett.*, **60**, 2937 (2006).
3. M. P. Proenca, C. T. Sousa, D.C. Leitao, J. Ventura, J.B. Sousa and J.P. Araujo, Nanopore formation and growth in phosphoric acid Al anodization, *J. Non-Cryst. Solids.*, **354**, 5238 (2008).
4. A. O. Araoyinbo, A. Rahmat, M. N. Derman and K. R. Ahmad KR, Room temperature anodization of aluminum and the effect of the electrochemical cell in the formation of porous alumina films from acid and alkaline electrolytes, *Adv. Mater. Lett*, **3,** 273 (2012).
5. U. Yogeswaran and S. M. Chen, A review on the electrochemical sensors and biosensors composed of nanowires as sensing material, *Sensors*, **8**, 290 (2008).
6. Z. Huang, W. Zhang, J. Yu and D. Gao, Nanoporous alumina membranes for enhancing hemodialysis, *J. Med. Device.*, **1**, 79 (2007).
7. A. M. Abd-Elnaiem and A. Gaber, Parametric study on the anodization of pure aluminum thin film used in fabricating nano-pores template, *Int. J.Electrochem. Sci*., **8**, 9741 (2013).
8. S. Altuntas, F. Buyukserin, Fabrication and characterization of conductive anodic aluminum oxide substrates, *Appl. Surf. Sci*., **318**, 290 (2014).
9. M. Jayalakshmi, K. Balasubramanian, Simple capacitors to supercapacitors an overview, *Int. J. Electrochem. Sci.*, **3**, 1196 (2008).
10. C. K. Chung, M. W. Liao, H. C. Chang and C. T. Lee, Effects of temperature and voltage mode on nanoporous anodic aluminum oxide films by one-step anodization, *Thin Solid Films*, **520**, 1554 (2011).
11. W. J. Stępniowski and Z. Bojar, Synthesis of anodic aluminum oxide (AAO) at relatively high temperatures. Study of the influence of anodization conditions on the alumina structural features, *Surf. Coat. Technol*., **206**, 265 (2011).
12. C. K. Chung, W. T. Chang, M. W. Liao, H. C. Chang and C. T. Lee, Fabrication of enhanced anodic aluminum oxide performance at room temperatures using hybrid pulse anodization with effective cooling, *Electrochim. Acta*., **56**, 6489 (2011).
13. D. Y. Hwang, Y. M. Kim and D. H. Shin, Corrosion resistance of plasma-anodized AZ91 Mg alloy in the electrolyte with/without potassium fluoride, *Mater. Trans.*, **50**, 671 (2009).
14. S. H. Su, C. S. Li, F. Bin. Zhang and M. Yokoyama, Characterization of anodic aluminum oxide pores fabricated on aluminum templates, *Superlattices Microstruct*., **44**, 514 (2008).
15. A. W. Juyana and M. N. Derman, Characterization of porous anodic aluminium oxide film on aluminium templates formed in anodizing process, *Adv. Mater. Res.*, **173**, 55 (2011).
16. Y. Jia, H. Zhou, P. Luo, S. Luo, J. Chen and Y. Kuang, Preparation and characteristics of well-aligned macroporous films on aluminum by high voltage anodization in mixed acid, *Surf. Coat. Technol*. **201**, 513 (2006).
17. G. D. Sulka and W. J. Stepniowski, Structural features of self-organized nanopore arrays formed by anodization of aluminum in oxalic acid at relatively high temperatures, *Electrochim. Acta*., **54**, 3683 (2009).
18. M. A. Kashi and A. Ramazani, The effect of temperature and concentration on the self-organized pore formation in anodic alumina, *J. Phys. D: Appl. Phys*., **38**, 2396 (2005).
19. S. M. J.Zaidi and M. Z. Butt, Designing low cost and low temperature electrochemical anodization

setup to obtain metal oxide templates, *Materials Today*: *Proceedings*, Elsevier, in press (2018).

20. J. W. Diggle, T. C. Downie and C. W. Goulding, Anodic oxide films on aluminum, *Chem.Rev*., **69**, 365 (1969).
21. Hariom, N. Verma, K. C. Singh, High field ionic conduction in anodic oxide films on tantalum in aqueous electrolytes, *Europ. J. Appl. Engg. Sci. Res.*, **2**, 25 (2013).
22. G. E. J. Poinern, N. Ali, D. Fawcett, Progress in nano-engineered anodic aluminum oxide membrane development, materials, **4**, 487 (2011).
23. S. Zhang, Y. Wang, Y. Tan, J. Zhu, K. Liu and J. Zhu, Anodic aluminum oxide with fine pore size control for selective and effective particulate matter filtering, *Mat. Res. Exp*., **3**, 074004 (2016).
24. C. S. Barret and T. B.Massalski, *Structure of Matals*, Pergamon, Oxford, p.204 (1980).
25. M. Z. Butt, D. Ali, M. Aftab and M. U. Tanveer, Surface topography and structure of laser-treated high purity zinc, *Surf. Topogr: Metrol.Prop*., **3**, 35002 (2015).
26. J. D. Makinson, J. S. Lee, S. H. Magner, R. J. De Angelis, W. N. Weins and A. S. Hieronymus, *Advances in X-ray Analysis* **42** 407 (2000).
27. G. K. Williamson, W. H. Hall, X-ray line broadening from filed aluminum and wolfram, *Acta Metall*, **1**, 22 (1953).
28. M. Z. Butt, M. W. Khaliq, A. M. Majeed and D. Ali, Impact of 532 nm 6 ns laser pulses on (104) oriented zinc single crystal: surface morphology, phase transformation, and structure hardness relationship, *Mat. Res. Exp*, **3**, 096503 (2016).
29. M. Z. Butt, A. M. Majeed, M. W. Khaliq, and Dilawar Ali, Structural, Electrical, and Mechanical Characterization of Al 5086 Alloy Irradiated with 248 nme20 ns KrF Excimer Laser, *J. Alloys Compounds*, **695**, 3069 (2017).
30. M. W. Khaliq, M. Z. Butt, and M. Saleem, Irradiation of zinc single crystal with 500keV singly-charged carbon ions: surface morphology, structure, hardness, and chemical modifcations, *Mater. Res. Express*, **4,** 076513 (2017).
31. T. Ungar, Microstructural parameters from X-ray diffraction peak broadening, *Scr. Mater*. **51**,777 (2004).